Discrete dipole approximation for calculating extinction and Raman intensities for small particles with arbitrary shapes

Wen-Hui Yang, George C. Schatz, and Richard P. Van Duyne
Department of Chemistry, Northwestern University, Evanston, Illinois 60208-3113

(Received 28 February 1995; accepted 14 April 1995)

We present a discrete dipole approximation (DDA) method to determine extinction and Raman intensities for small metal particles of arbitrary shape. The Raman intensity calculation involves evaluation of surface electromagnetic fields, and thus is relevant to surface enhanced Raman scattering (SERS) intensities. We demonstrate convergence of the method by considering light absorption and scattering from an isolated spheroid, from an isolated tetrahedron, from two coupled spheroids, and from a spheroid on a flat surface. We also examine comparisons with traditional T-matrix methods. Extensions and simplifications of the method in studies of clusters and arrays of particles are presented. © *1995 American Institute of Physics.*

I. INTRODUCTION

Recent advances in nanofabrication technology have made it possible to prepare small ($<$100 nm) metal particles (isolated particles, clusters, and arrays of particles) with controllable and reproducible shapes (approximately spheroids, tetrahedrons, triangular, and hexagonal prisms).[1] These particles have been characterized using a variety of optical methods, including absorption spectroscopy and surface enhanced raman scattering (SERS), and by structural probes like AFM and STM. A variety of size and shape dependent results are found in the optical studies that relate to surface plasmon excitation, such as peaks in absorption and Raman excitation profiles, and for the case of noble metal particles, significant enhancements in Raman intensities.[2] In principle, all of these measurements should be capable of quantitative theoretical analysis in which the measured AFM or STM structural information is input to a solution of Maxwell's equations, and then absorption and Raman intensities are calculated based on known dielectric properties. However this analysis has not been performed so far, in part because solving Maxwell's equations accurately for particles other than spheres is a numerically tedious process.[3] The difficulty is especially serious for particles with sharp points because of strong field gradients.

In this paper we show that it is possible to use a method known as the discrete dipole approximation (DDA) to determine the desired spectroscopic information for small metal particles of arbitrary shape. The DDA was first developed in the field of astrophysics by Purcell and Pennypacker,[4] and has proved to be a powerful tool in studies of light scattering from nonmetallic dust particles of astrophysical interest.[5,6] The discrete dipole (or coupled dipole) approximation involves replacing each particle by an assembly of finite cubical elements, each of which is small enough that only dipole interactions with an applied electromagnetic field and with induced fields in other elements need to be considered. This reduces the solution of Maxwell's equations to an algebraic problem involving many coupled dipoles. In fact, with an appropriate choice of dipole polarizability for each element,[7] the electric fields determined by the DDA will match the Maxwell equation results quantitatively in the limit of a large enough number of elements. Very efficient methods for solving the DDA equations have been developed[8] using fast fourier transform[9] and complex-conjugate gradient methods, and as a result it is possible to use thousands of dipoles for routine calculations, and many tens of thousands of dipoles for benchmark studies.

Typically the DDA has been applied to isolated particles whose refractive index is close to unity, and whose size is comparable to or less than the wavelength of visible light. In addition, only far-field information such as the absorption cross section has been determined. In the present paper we show that this method can be applied very efficiently to problems involving small metal particles (having complex dielectric constants which are much larger than unity in magnitude), and to the determination of SERS intensities (requiring near-field information). We also show that it may be applied to assemblies of particles, and to particles that are near to a flat surface. The near-field calculation is especially challenging, as sensitivity to the discretization used in reducing the object to an assembly of dipoles could be significant. Substrate effects have been considered in past DDA studies,[10] but it remains to be seen if this approach can easily be used to study SERS active particles adsorbed onto flat substrates (a typical configuration for SERS experiments). The specific particles that we consider are based on recent experiments with silver particles,[1,2] but our focus will be on testing theoretical methods rather than experimental modeling.

To provide a reference for our DDA results, we will compare with calculations from two previously developed methods, one based on numerical solutions of Maxwell's equations[3] (the so-called T-matrix method[11]), and the other an analytical theory known as the modified long wavelength approximation (MLWA).[12,13] The T-matrix results represent numerically exact but computationally tedious solutions of Maxwell's equations. Because of the computational difficulties associated with such calculations, only a few results have been presented in past work.[3] The MLWA is based on analytical solutions to the Poisson equation (i.e., infinite wavelength limit of Maxwell's equations) with corrections for finite wavelength effects that are described through order $(R/\lambda)^3$ where R is the particle size and λ is the wavelength.

Corrections are also made for the size dependence of the metal dielectric constant that arises for particles that are smaller than the conduction electron mean free path. For spheroids that are not too prolate or oblate, the electric field enhancements obtained from the MLWA match T-matrix results quite well near the primary plasmon peak.[12] The MLWA is also simple to use, so it has been applied extensively in studies of Raman and second harmonic enhancements.[12,13] However, the MLWA is limited in its ability to describe arbitrarily shaped particles, and even for spheroids its accuracy deteriorates for the highly oblate or prolate objects that are often of most interest to SERS studies.

II. THEORY

A. Discrete dipole approximation

The DDA starts by dividing the object of interest into a cubic array of N-point dipoles whose positions are denoted $\mathbf{r}_i$, with polarizabilities α_i. The polarization induced in each dipole as a result of interaction with a local electric field $\mathbf{E}_{\rm loc}$ will be (omitting the frequency factors $e^{i\omega t}$),

$$\mathbf{P}_i = \boldsymbol{\alpha}_i \cdot \mathbf{E}_{\rm loc}(\mathbf{r}_i). \tag{1}$$

$\mathbf{E}_{\rm loc}$, for isolated particles, is the sum of an incident field and a contribution from all other dipoles in the same particle,

$$\mathbf{E}_{\rm loc}(r_i) = \mathbf{E}_{{\rm loc},i} = \mathbf{E}_{{\rm inc},i} + \mathbf{E}_{{\rm self},i} = \mathbf{E}_0 \exp(i\mathbf{K}\cdot\mathbf{r}_i) - \sum_{j\neq i} \mathbf{A}_{ij}\cdot\mathbf{P}_j . \tag{2}$$

$\mathbf{E}_0$ and $\mathbf{K}$ are the amplitude and wave vector of the incident wave, respectively, and the interaction matrix $\mathbf{A}$ has the following form:

$$\mathbf{A}_{ij}\cdot\mathbf{P}_j = \frac{\exp(ikr_{ij})}{r_{ij}^3}\left\{ k^2 \mathbf{r}_{ij}\times(\mathbf{r}_{ij}\times\mathbf{P}_j) + \frac{(1-ikr_{ij})}{r_{ij}^2} \times [r_{ij}^2\mathbf{P}_j - 3\mathbf{r}_{ij}(\mathbf{r}_{ij}\cdot\mathbf{P}_j)] \right\} \quad (j\neq i), \tag{3}$$

where $k=\omega/c$.

If the system of interest consists of many metal particles on top of a flat substrate, $\mathbf{E}_{{\rm loc},i}$ will have additional contributions, including a field $\mathbf{E}_{{\rm ref},i}$ arising from reflection of the incident field from the substrate, a field $\mathbf{E}_{{\rm others},i}$ due to fields from dipoles on other particles (the interparticle interaction) and a field $\mathbf{E}_{{\rm subs},i}$ from reflection of dipole radiation due to all the particles from the substrate (the substrate effect). Thus in the more general case the local field is

$$\mathbf{E}_{{\rm loc},i} = \mathbf{E}_{{\rm inc},i} + \mathbf{E}_{{\rm ref},i} + \mathbf{E}_{{\rm self},i} + \mathbf{E}_{{\rm others},i} + \mathbf{E}_{{\rm subs},i}, \tag{4}$$

where

$$\mathbf{E}_{{\rm ref},i} = F_{\parallel,\perp}\mathbf{E}_0 \exp(\mathbf{K}'\cdot\mathbf{r}_i),$$

$$\mathbf{E}_{{\rm others},i} = -\sum_{j'}{}' \mathbf{A}_{ij'}\cdot\mathbf{P}_{j'}, \tag{5}$$

$$\mathbf{E}_{{\rm subs},i} = -\sum_{j'} \mathbf{A}_{ij'}\cdot\mathbf{P}''_{j'}.$$

In Eq. (5), the field $\mathbf{E}_{{\rm ref},i}$ includes the Fresnel coefficient F[14] for either parallel or perpendicular polarization, and the wave vector of the reflected field is denoted $\mathbf{K}'$. Note that the fourth term in Eq. (4) includes the contribution of other particles, i.e., sums over all dipoles except those on the same particle as i [hence the prime on the sum in Eq. (5)], while the last term, the substrate effect, includes contribution from all dipoles including i. For both these terms, the interaction matrix is given by Eq. (3).

As an approximation for $\mathbf{E}_{{\rm subs},i}$, one can use the classical image model,[15] in which the field arising from a dipole moment $\mathbf{P}_j$ located at $\mathbf{r}_j=(x_j,y_j,z_j)$ due to polarization of the substrate is assumed to be given by a dipole moment $\mathbf{P}''_j$ located at $\mathbf{r}''_j = (x_j, y_j, -z_j)$ (where z_j measures the distance from the surface), given by

$$\mathbf{P}''_{\parallel j} = -\frac{\epsilon_{\rm subs}-1}{\epsilon_{\rm subs}+1}\mathbf{P}_{\parallel j}, \quad \mathbf{P}''_{\perp j} = \frac{\epsilon_{\rm subs}-1}{\epsilon_{\rm subs}+1}\mathbf{P}_{\perp \mathbf{j}}, \tag{6}$$

and where $\epsilon_{\rm subs}$ is the substrate dielectric constant. Equation (6) is an approximation for the reflected waves associated with a dipole near a dielectric surface that was previously derived (along with more rigorous theory) in Ref. 9. In this study, it was found that the image model expression becomes accurate either when the dipoles are close to the surface, or when the surface is a good reflector. Both of these restrictions are generally satisfied for the kind of problems we are interested in, so the image approximation should not be a serious source of error in this situation.

Equations (3) and (6) are appropriate for metal particles in vacuum, but it is not difficult to generalize them to consider particles in a dielectric medium. Note that the number of dipoles is not increased as a result of substrate interactions in the image approximation.

Substituting Eqs. (4) or (5) into Eq. (1) and rearranging terms in the equation, we generate an equation of the form

$$\mathbf{A}'\cdot\mathbf{P} = \mathbf{E}, \tag{7}$$

where $\mathbf{A}'$ is a matrix which is built out of the matrix $\mathbf{A}$ from Eq. (3). For a system with a total of N dipoles, $\mathbf{E}$ and $\mathbf{P}$ in Eq. (7) are $3N$-dimensional vectors, and $\mathbf{A}'$ is a $3N\times 3N$ matrix. By solving these $3N$ complex linear equations, polarization vectors are obtained, and with these, optical cross sections, local fields and Raman enhancements can be calculated.

B. Clusters and periodic arrays of identical particles

In some of the recent experiments,[1,2] large clusters and periodic arrays of identical particles were prepared on a dielectric substrate. The distance between these particles is variable, but in many cases they are too close to be able to neglect their mutual interactions. It is possible, however, to use the DDA to describe these clusters and arrays, either by locating dipoles on all the particles and letting them interact, or by having dipoles on only one particle, and using the following approximation for the induced polarization of dipoles in the other particles:

$$\mathbf{P}(\mathbf{r}_a) = \mathbf{P}_0 \exp(i\mathbf{K}\cdot\mathbf{r}_a), \tag{8}$$

where $\mathbf{P}_0$ is the polarization of each dipole in the particle at the origin, and $\mathbf{r}_a$ an integer multiple of the lattice vector that locates the ath particle.

This periodic polarization (PP) expression for $\mathbf{P}(\mathbf{r}_a)$ follows from a close inspection of Eq. (4) for the case of two identical dipoles in different lattice sites but in otherwise equivalent locations. Substituting Eq. (8) into Eq. (4) for dipoles that are on the particle at $\mathbf{r}_a$, one finds a result which is identical to Eq. (4) for the particle at $\mathbf{r}_0$ except for parts of the fourth and fifth terms (the interparticle interactions). So, this approximation requires that interactions between dipoles on the *same* particles be larger than between dipoles on *different* particles, something which is satisfied if the particles are far enough apart. If the particles are too close, and the terms are comparable, then the result will deviate from the exact result. In the next section, we will see how much the PP approximation deviates from exact DDA for the case of a two particle array.

C. Cross sections and Raman enhancement

Extinction and absorption cross sections are taken from the optical theorem[16] and have the following forms:

$$C_{\text{ext}}=\frac{4\pi k}{|\mathbf{E}_0|^2}\sum_{j=1}^{N}\ \text{Im}(\mathbf{E}^*_{\text{inc},j}\cdot\mathbf{P}_j), \tag{9}$$

$$C_{\text{abs}}=\frac{4\pi k}{|\mathbf{E}_0|^2}\sum_{j=1}^{N}\left\{\text{Im}[\mathbf{P}_j(\alpha_j^{-1})^*\mathbf{P}_j^*]-\frac{2}{3}k^3|\mathbf{P}_j|^2\right\}. \tag{10}$$

The scattering cross section is equal to $C_{\text{ext}}-C_{\text{abs}}$.

The electromagnetic contribution to the SERS intensity can be determined by evaluating the local field $\mathbf{E}_{\text{loc},i}(\omega)$ on the exposed surfaces of each of the cubes using Eq. (4). The electromagnetic field enhancement factor $F(\omega)$ is then determined by averaging the square of $\mathbf{E}_{\text{loc},i}(\omega)$ over the exposed surfaces, and normalizing by the incident field, i.e.,

$$F(\omega)=\frac{\langle|\mathbf{E}_{\text{loc},i}(\omega)|^2\rangle}{\mathbf{E}_0^2}, \tag{11}$$

where the bracket is used to denote the surface average, as defined further below. A commonly used expression for the SERS enhancement factor[13] involves multiplying field enhancement factors for the incident and Stokes shifted frequencies, ω and ω', i.e.,

$$R(\omega,\omega')=F(\omega)F(\omega'). \tag{12}$$

This expression is only an approximation to the true Raman enhancement factor (valid in the limit that the particle size is small compared to the wavelength λ), but tests of its accuracy suggest that it is adequate for the problems we are considering.[17] Note that the field and Raman enhancement factors that we have defined refer to molecules located on the exposed surfaces of the cubical elements. A quadrature involving typically 20 points randomly scattered over each exposed surface of each cube gives a convergent result for the problems that we have considered. These exposed cube surfaces are only an approximation to the surfaces of smooth particles such as spheres and spheroids, so we have also considered evaluating the field on the smooth surface, still using the local field $\mathbf{E}_{\text{loc},i}$ associated with the coupled dipoles. Later we present comparisons of these two different ways to evaluate the field.

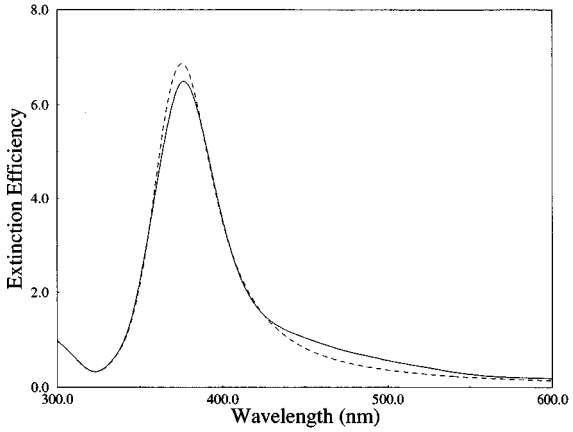

FIG. 1. DDA extinction efficiency vs wavelength for a spheroidal particle. Solid line, 384 dipoles; dashed line, 2968 dipoles.

III. CALCULATIONS

To test the DDA approach in applications to silver particles we consider four specific examples; an isolated oblate spheroid, an isolated tetrahedron, two coupled identical oblate spheroids, and an oblate spheroid next to a flat substrate. Unless otherwise stated, we use dielectric constants appropriate for silver from Ref. 18. The isolated spheroid is assumed to have a major axis of 50 nm and a minor axis (the axis of revolution) 35 nm, while the height of each face of the tetrahedron is taken to be 50 nm, which makes the edge length be 57.7 nm. For the coupled spheroids, the major axes are assumed collinear, with the separation between the closest tips taken to be a parameter that we vary from zero to infinity. The laser polarization is assumed parallel to the spheroid major axis in all these calculations. The spheroid next to a flat substrate is identical in properties to the isolated spheroid, with its minor axis perpendicular to the substrate, the applied field assumed to be parallel to the surface, and the substrate assumed to be mica with $\epsilon_{\text{subs}}=2.55$.

In solving the complex linear equations [Eq. (7)] for the induced polarizations, we have adapted a program from Draine and Flatau,[8] which uses fast fourier transform (FFT) and complex-conjugate gradient methods[9] to facilitate treatment of a very large number of dipoles ($>10^4$). The polarizability of each dipole is assumed to follow the lattice dispersion relation (LDR) proposed by Draine and Goodman.[7] This insures that the correct Maxwell equation solution will be obtained in the limit of a large number of dipoles.

IV. RESULTS AND DISCUSSION

Figure 1 shows the extinction efficiency of the isolated spheroid as a function of wavelength, comparing results for 384 and 2968 dipoles. Extinction efficiency is the ratio of the extinction cross section to effective particle area where the latter is defined as the area of a sphere with the same volume as the particle. Figure 2 shows the corresponding results for the Raman enhancement factor (with an assumed Stokes shift of 1650 cm^{-1}). In both Figs. 1 and 2, we see a

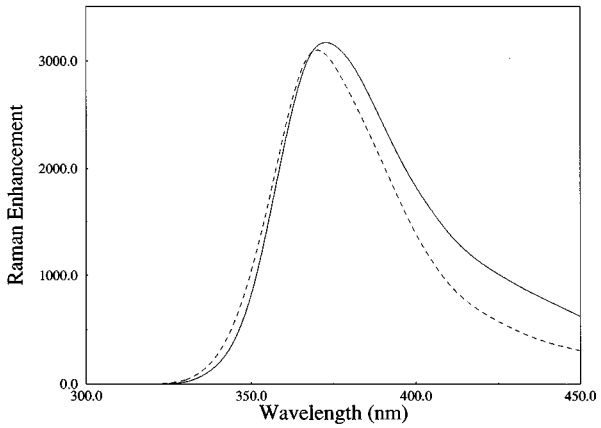

FIG. 2. Raman enhancement vs wavelength for the same particle parameters as in Fig. 1.

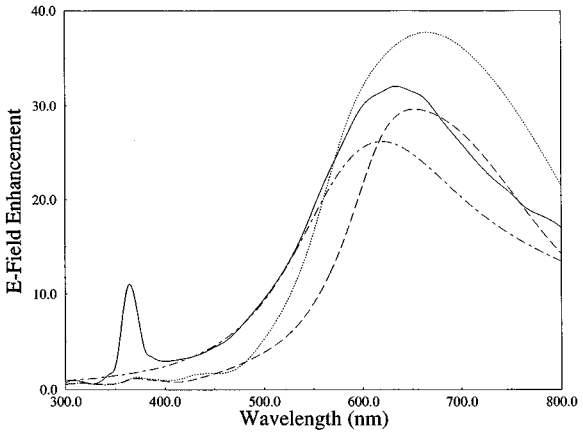

FIG. 4. Electric field enhancement factor vs wavelength for a prolate spheroid having a major axis of 200 nm and an aspect ratio of 2:1. The results include a T-matrix result from Barber *et al.* (solid), DDA with rough surface (dotted), DDA with exact spheroid surface (dashed), and MLWA (dash–dot).

typical plasmon excitation resonance profile, with good agreement between results for the different dipole numbers. The Raman enhancement factor calculation provides an especially severe test of the method, as the surface fields are significantly larger (factor of >10) than the incident field. Fortunately, the convergence with respect to dipole number is good, indicating that fluctuations in the surface fields due to the contributions of nearby dipoles are not a serious hindrance.

Figure 3 compares extinction results for the isolated spheroid based on DDA calculations for 2968 dipoles with the corresponding results of T-matrix and MLWA calculations that we have done. Figure 4 presents the corresponding information for the electric field enhancement factor $F(\omega)$ [see Eq. (11)]. For Fig. 4 only, the results refer to *prolate* spheroid calculations with parameters taken from Ref. 3 (major axis$=$200 nm, minor axis$=$100 nm), and with a dielectric constant taken from Ref. 19. Included in Fig. 4 are T-matrix results from Ref. 3, MLWA results that we have calculated, and two DDA results, one based on the exposed cube (rough) surfaces, and the other based on the exact (smooth) surface of the spheroid. The results presented in Figs. 3 and 4 show reasonable agreement between all three theories, with $<20\%$ deviations in the peak intensity relative to the T-matrix result. The rough and smooth surface DDA results are in more or less comparable agreement with the T-matrix, indicating that the method for performing the surface average is not that important. Since the rough surface DDA generalizes more easily to arbitrary shaped objects, we will use this is subsequent work. Note that neither the DDA nor MLWA results describe the small peak at 360 nm, which Barber *et al.*[3] ascribe as arising from a quadrupole resonance. This result is consistent with the idea that the DDA and MLWA theories are based on dipole fields, and thus will not describe quadrupolar resonance features.

Figures 5 and 6 show extinction and Raman enhancement results for the tetrahedron, comparing 1622 and 2321 dipoles. Here we see multiple plasmon peaks, with the most intense features being strongly red-shifted compared to the corresponding spheroid peaks in Figs. 1 and 2. In addition, the extinction and Raman excitation profiles are different, with the Raman enhancements being large at longer wave-

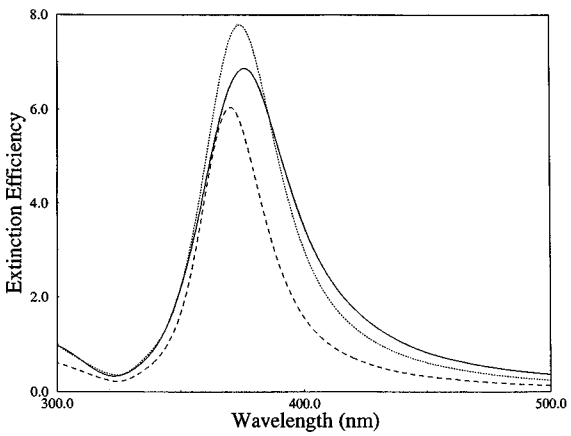

FIG. 3. Extinction efficiency vs wavelength for spheroid of Fig. 1 from DDA (solid), MLWA (dotted), and T-matrix (dashed) calculations.

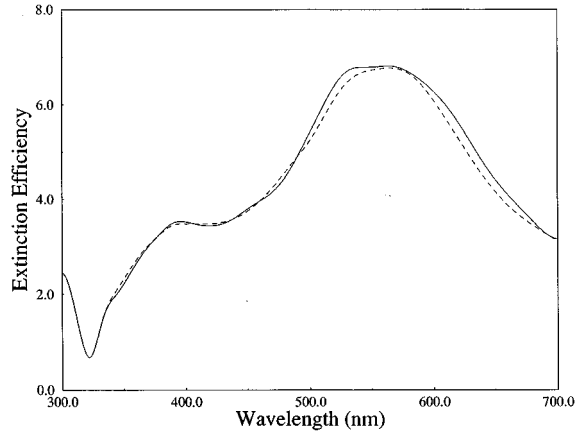

FIG. 5. DDA extinction efficiency vs wavelength for a tetrahedron. Solid line, 2321 dipoles, dashed, 1622 dipoles.

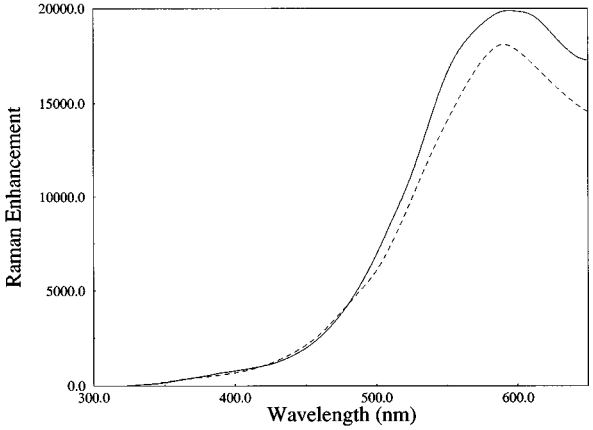

FIG. 6. Raman enhancement vs wavelength for the same particle as in Fig. 5.

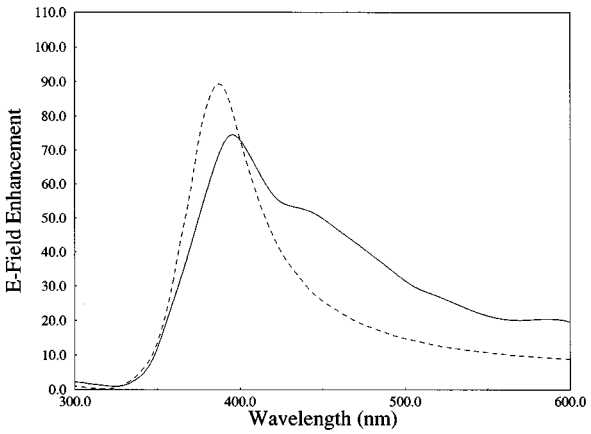

FIG. 8. Electric field enhancement of the same system as in Fig. 7. Here the solid curve shows both the full and PP DDA, and the dashed curve shows MLWA.

lengths than the corresponding peak extinction. Again there is very good correspondence between the results for the different dipole numbers. This shows that the sharp points on the tetrahedron do not severely impact convergence of the DDA.

Now consider the two spheroid system. Figures 7 and 8 present extinction and electric field enhancements for this case, with the spheroid separation taken to be $1\times$ the semimajor axis. The results shown were obtained by the following methods:

(i) Full DDA, in which each spheroid is represented by 384 dipoles, and all dipoles are fully coupled.
(ii) Decoupled DDA, in which the DDA is first applied to each particle, and then the total dipoles on the two spheroids are coupled.
(iii) PP-DDA, in which Eq. (8) is invoked to eliminate half of the dipoles.
(iv) MLWA for each spheroid, with dipole coupling between the overall dipole on each spheroid.

Figures 7 and 8 show that methods (i) and (iii) are in excellent correspondence, being barely distinguishable on the scale of the plot. Method (ii) is less quantitative, so since this involves comparable effort compared to (iii), i.e., the same number of dipoles, method (iii) is to be preferred. Method (iv) is also less quantitative, but involves negligible computational effort compared to the others, so it might be useful for qualitative work.

Figures 9 and 10 show extinction and electric field enhancement results for the two coupled spheroids as a function of separation, including results varying from infinite separation (where one recovers the isolated spheroid result), to zero separation (where the spheroids touch). The full DDA, with 384 dipoles on each spheroid, was used for these calculations. Both figures show the expected red-shifting in the plasmon energy as the spheroids approach, with relatively small changes in the results until the spheroids touch. The zero separation limit leads to complex extinction and electric field enhancement profiles, suggesting multiple overlapping plasmon resonances. We have also performed PP-

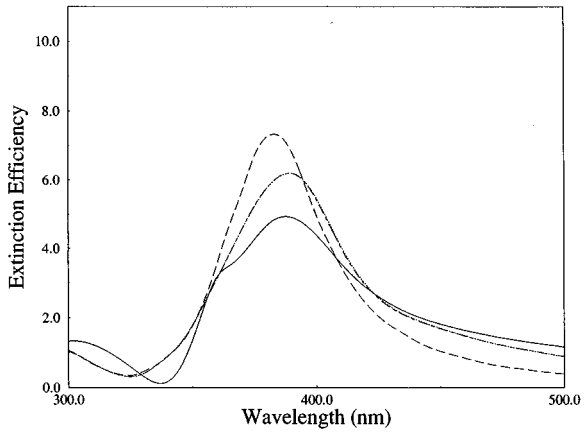

FIG. 7. Extinction efficiency vs wavelength for two spheroidal particles with a separation $1\times$ semimajor axis, obtained by the following methods: (i) full DDA (dotted), (ii) decoupled DDA (solid), (iii) PP DDA (dot–dash), and (iv) MLWA (dashed).

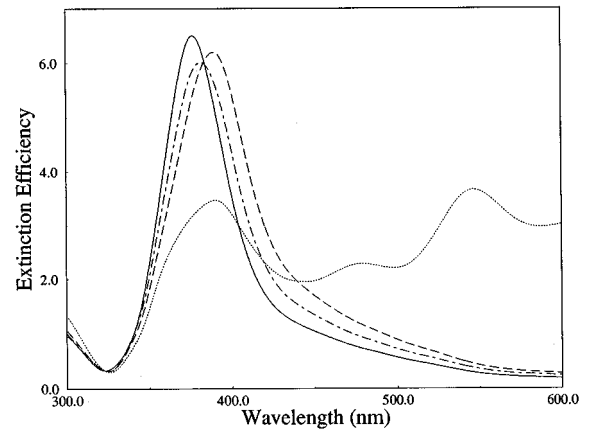

FIG. 9. Extinction efficiency vs wavelength for two spheroidal particles, with varying separation, obtained by full DDA. Separation between the particles is as follows: (i) infinite (solid curve), (ii) $2\times$ semimajor axis (dot–dash), (iii) $1\times$ (dashed), (iv) zero (dotted).

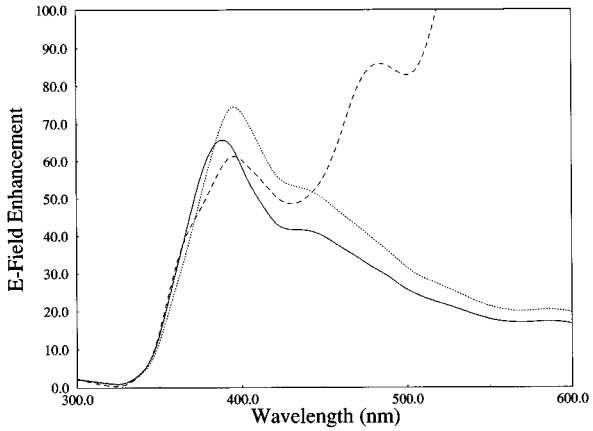

FIG. 10. Electric field enhancement vs wavelength for the same system as in Fig. 9. Separation between particles is (i) 2× semimajor axis (solid), (ii) 1× (dotted), and (iv) zero (dashed).

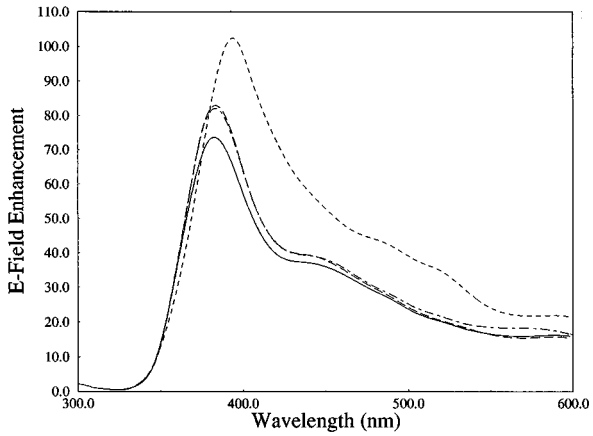

FIG. 12. Electric field enhancement vs wavelength for the same system as in Fig. 11.

DDA calculations for spheroid geometries which match those in Figs. 9 and 10, and we find that the results match the DDA results accurately for all spheroid separations except zero separation. Even for zero separation the error in the extinction and electric field is never larger than a factor of 2.

Figures 11 and 12 show extinction and field enhancement for the oblate spheroid/mica surface system. Again we see red shifting as the particle approaches the surface, but the effect is less dramatic than for the coupled spheroids. The **E** field increases most noticeably when the spheroids touch, but the effect is still modest.

V. CONCLUSION

The present results show that the DDA can be applied to the interaction of electromagnetic fields with small metal particles of relevance to recent nanofabrication experiments. Specifically we have shown that the DDA extinction spectra and Raman enhancements converge with increasing dipole number for representative spheroidal and tetrahedral particles and for two coupled spheroids. The number of dipoles needed to produce accurate results in these examples is small enough that calculations at many wavelengths or for many particles or for more complex particle shapes are possible. We have also demonstrated that for arrays or clusters of particles it is possible to reduce the number of coupled dipoles using Eq. (8).

To verify the accuracy of our DDA results, we have considered the comparison of DDA, T-matrix, and MLWA results. Such comparisons are only possible for spheroids, but at least in this case we find results that are in reasonable agreement. Our T-matrix calculations were much more time consuming than DDA, so it is encouraging to see that one can use DDA to generate results of equivalent quality using less computational resources. The MLWA method is much simpler still, but it is also much more limited than DDA in its range of applicability. Finally, we have described how the DDA may be used for metal particles near to a flat surface. This should be of relevance to our future work in this area which is aimed at quantitative modelling of nanofabrication experiments which produce such configurations of particles.

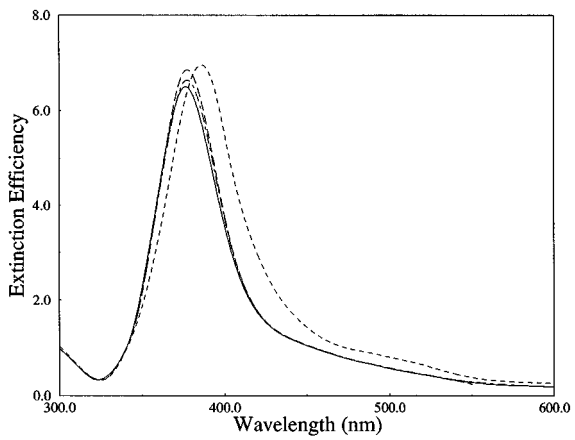

FIG. 11. Extinction efficiency vs wavelength for a spheroid particle next to a mica substrate. Distances between particle and substrate are (i) zero (dashed), 1× semiminor axis (long-dash), (iii) 2× (dot–dash), (iv) infinite (solid).

ACKNOWLEDGMENTS

We thank A. C. R. Pipino, D. Treichel, J. Hulteen, and especially S. P. Druger for valuable comments. Initial stages of this research were supported by NSF Grant No. DMR-8802706.

[1] R. P. Van Duyne, J. C. Hulteen, and D. A. Treichel, J. Chem. Phys. **99**, 2101 (1993); J. C. Hulteen and R. P. Van Duyne, J. Vac. Sci. Technol. A (in press).
[2] W. B. Caldwell, K. Chen, B. R. Herr, C. A. Mirkin, J. C. Hulteen, and R. P. Van Duyne, Langmuir **10**, 4109 (1994).
[3] P. W. Barber, R. K. Chang, and H. Massoudi, Phys. Rev. B **27**, 7251 (1983).
[4] E. M. Purcell and C. R. Pennypacker, Astrophys. J. **186**, 705 (1973).
[5] B. T. Draine, Astrophys. J. **333**, 848 (1988).
[6] B. T. Draine and P. J. Flatau, J. Opt. Soc. Am. A **11**, 1491 (1994).
[7] B. T. Draine and J. J. Goodman, Astrophys. J. **405**, 685 (1993).
[8] Program DDSCAT, by B. T. Draine and P. J. Flatau, University of California, San Diego, Scripps Institute of Oceanography, 8605 La Jolla Dr., La Jolla, California 92093-0221.
[9] J. J. Goodman, B. T. Draine, and P. J. Flatau, Opt. Lett. **16**, 1198 (1991).
[10] M. A. Taubenblatt and T. K. Tran, J. Opt. Soc. Am. A **10**, 912 (1993).

[11] P. W. Barber and S. C. Hill, *Light Scattering by Particles: Computational Methods* (World Scientific, Singapore, 1990).
[12] E. J. Zeman and G. C. Schatz, in *Dynamics of Surfaces, Proceedings of the 17th Jerusalem Symposium*, edited by B. Pullman, J. Jortner, B. Gerber, and A. Nitzan (Reidel, Dordrecht, 1984), p. 413.
[13] E. J. Zeman and G. C. Schatz, J. Phys. Chem. **91**, 239 (1987).
[14] M. Born and E. Wolf, *Principles of Optics*, 6th ed. (Pergamon, Oxford, 1989).
[15] T. Yamaguchi, S. Yoshida, and A. Kinbara, Thin Solid Films **21**, 173 (1974).
[16] C. F. Bohren and D. R. Huffman, *Absorption and Scattering of Light by Small Particles* (Wiley–Interscience, New York, 1983).
[17] M. Kerker, J. Colloid Interface Sci. **118**, 417 (1987).
[18] H. J. Hagemann, W. Gudat, and C. Kunz, J. Opt. Soc. Am. **65**, 742 (1975).
[19] P. B. Johnston and R. W. Christy, Phys. Rev. B **6**, 4370 (1968).